The Influence of Protein Environment on the Low Temperature Electronic Spectroscopy of Zn-Substituted Cytochrome *c*

Eric S. Manas,[†,‡] Wayne W. Wright,[‡] Kim A. Sharp,[‡] Josef Friedrich,[§] and Jane M. Vanderkooi*[,†]

Johnson Research Foundation, Department of Biochemistry and Biophysics, University of Pennsylvania School of Medicine, Philadelphia, Pennsylvania 19104-6059, and Technische Universität München, Lehrstuhl für Physik Weihenstephan, Vöttinger Strasse 40, D-85350 Freising, Germany

Received: February 14, 2000; In Final Form: May 10, 2000

Low-temperature UV−vis absorption and Stark-effect hole-burning spectra of Zn substituted cytochrome *c* are studied experimentally and theoretically using quantum mechanical and Poisson−Boltzmann electrostatics models. Both the Q and Soret bands show resolved splitting at temperatures below ∼180 K. The trend observed in the splittings when comparing cytochromes from different species is found to be the same as that observed for the Q(0,0) band of ferrous cytochrome *c*. The relative magnitudes of the Q and Soret splittings are found to be consistent with predictions based on Gouterman's four orbital model. For horse heart and yeast cytochrome *c*, which show the greatest difference in the UV−visible band splittings, Stark effect measurements on persistent spectral holes in the Q(0,0) band indicate that the protein-induced polarization is distinctly different for these two species. Incorporation of the protein electrostatic field as virtual point charges into quantum mechanical calculations utilizing the INDO/s semiempirical Hamiltonian is used to demonstrate that the effects of the protein on the heme electronic structure can be considerably different for the two proteins, consistent with the experimental observations.

I. Introduction

Porphyrin electronic transitions in heme proteins provide a useful tool for probing the protein environment. This is due to the high susceptibility of the porphyrin π-electron cloud to perturbations by the surrounding protein. These perturbations can arise from structural distortions of the porphyrin ring,[1−8] from the internal electric field generated by charged and polar groups[9−16] or from axial ligation to the heme iron by one or more amino acid residues.[9−17]

The UV−vis absorption spectrum of ferrous cytochrome *c* (cyt *c*) consists of three main bands: the Q(0,0) band or α-band just above 18000 cm^{-1}, and the B(0,0) or Soret band just above 24000 cm^{-1}, both of which are considered to be purely electronic transitions involving the porphyrin ring of the heme group, and the Q(0,1) band or β-band, which is just above the Q(0,0) band and is considered to be composed of many vibronic transitions.[18] It has been known for a long time that the Q(0,0) band of Fe(II) cyt *c* and other heme proteins shows splitting, either at room temperature, or as the temperature is lowered.[19−31] For example, the Q(0,0) band of horse heart Fe(II) cyt *c* shows resolved Q(0,0) splitting below 180 K.[25] The reason for this splitting is typically attributed to a reduction in molecular symmetry due to the surrounding protein, leading to a removal of the double degeneracy of the porphyrin e_g symmetry LUMO and hence a Q-band splitting. This reduction in symmetry has also been suggested by EPR,[32] Raman,[21,33−35] and spectral hole burning,[13,36] as well as by computational simulations.[13] Finally, a recent study by Manas et al.[22] suggested that the trend observed in the Q(0,0) splitting when comparing different species of cyt *c* could be attributed to the way the protein internal electric field interacts with the porphyrin ring, with contributions due to the protein-induced distortion of the ring.

The Zn substituted analogue of cyt *c* has been used instead of Fe(II) cyt *c* with techniques such as photochemical hole-burning or line-narrowed fluorescence, since the former exhibits a longer excited state lifetime and is strongly fluorescent. On the basis of NMR data it has been suggested that substitution with Zn does not significantly alter the protein structure in the vicinity of the heme pocket.[37] Consistent with the nativelike structure for the Zn derivative, it has been shown that photo-activated Zn derivatives of cyt *c* can donate electrons to neighboring proteins that also react with the native ground-state protein.[38,39] As will be demonstrated below, both the Q and Soret bands of Zn cyt *c* show splitting at low temperature. However, it has yet to be shown whether the splittings follow the same trend as Fe(II) cyt *c* when comparing different species. If this is the case, then this would present further evidence that substituting Zn(II) for Fe(II) does not significantly perturb the protein structure. Furthermore, because of the long lifetime of the excited singlet state, it is possible to carry out hole burning experiments, and the Stark effect on spectral holes burnt into the Zn cyt *c* absorption spectrum can also be compared for different species, and this can be used to gain insight into the origin of the band splitting.

In a previous study,[22] hereafter referred to as I, using combined quantum mechanical and Poisson−Boltzmann (PB) electrostatics models, we demonstrated that the Q(0,0) band splitting for a series of cytochrome *c* proteins from different species could be explained by a combination of heme distortion and interaction of the heme charge distribution with the heme pocket electric field.[22] These combined effects were shown to lead to porphyrin ring symmetry reduction, which results in a

* To whom correspondence should be addressed. Phone: 215-898-8783. E-mail: vanderko@mail.med.upenn.edu.
† Present address: Wyeth-Ayerst Research, 145 King of Prussia Road, Radnor, PA 19087.
‡ Johnson Research Foundation.
§ Technische Universität München.

10.1021/jp0005975 CCC: $19.00
Published on Web 07/01/2000

splitting of the degeneracy of the transition. Since the majority of the internal field strength originates from near-field monopolar and dipolar (i.e., the propionic acid peripheral groups and the axial ligands his18† and met80†) effects, we showed that the internal field is highly nonuniform, and that the porphyrin ring symmetry reduction cannot be explained in terms of the traditional uniform field Stark effect. We circumvented this problem by using a multipole expansion for the macrocycle charge distribution, truncating at the quadrupole term as a first approximation. The interactions between the porphyrin dipole/quadrupole moments and the internal field/field gradients were then incorporated into a five-level model (derived from Gouterman's four-orbital model) in order to explain the observed trends in splitting.

The model in I[22] utilized the fact that the electronic structure of the porphyrin ring is well understood in terms of Gouterman's four-orbital model.[18,40] The interaction with the protein electric field was treated using a multipolar expansion in order to give a simplified picture of how the protein electrostatic field influences the porphyrin ring. This study served to highlight the key factors that are likely to lead to Q(0,0) band splitting, but we felt more detailed modeling is necessary in order to more quantitatively include the contribution of these factors to the porphyrin ring electronic structure and spectral properties. Hence, in this paper, the electronic structure calculations on the distorted porphyrin ring structure of the proteins utilize the intermediate neglect of differential overlap method parametrized for spectroscopy (INDO/s) by Zerner and co-workers.[41−43] The singles-configuration interaction (SCI) method is used in conjunction with the INDO/s Hamiltonian to compute the excited-state properties. Electrostatic effects are then incorporated into the INDO/s-SCI calculations by fitting the internal field obtained from Poisson−Boltzmann calculations to a set of virtual point charges, and including these charges in the Fock matrix as a sum of unshielded Coulombic potential functions.

Our goals are as follows. First, we will show that the Zn substituted analogues of cyt *c* from different species (horse heart, tuna heart, and yeast cyt *c*) show low-temperature splittings in both the Q and Soret bands. We then intend to demonstrate that the relative magnitudes of the Q and Soret splittings for a given species, as well as in comparing different species, are consistent with the model presented in I.[22] Finally, we present the results of Stark effect hole burning measurements on horse heart and yeast cyt *c*. Using the combined INDO/s-SCI−PB model described above, we will show that the difference in the Stark effect between the two proteins can be attributed to the way the protein polarizes the porphyrin ring of the heme.

This paper is organized as follows. In section II, experimental procedures and our method for performing combined quantum mechanical/classical electrostatic modeling are described. In the following section, the low-temperature absorption spectra for horse heart, tuna heart, and yeast cyt *c* are given. In section IV, Stark-effect holeburning spectra are presented for horse heart and yeast Zn cyt *c*, and the results are compared with the trend observed for the splitting. In the next Section, combined INDO/s-SCI−PB are presented for the proteins, and used to help interpret the experimental results. A discussion and conclusions appears in the final section.

II. Materials and Methods

Experimental Methods. Cyt *c* from horse heart, yeast (Saccharomyces cervesiae), and tuna were obtained from Sigma Chemical Co. (St. Louis, MO). The iron was replaced by zinc using previously described methods.[44] Yeast cyt *c* contains a free sulfhydral group. Therefore, to maintain this group reduced, 2 mM dithiothreitol was added to the buffer during the column purification. The purified protein samples were stored in 50% glycerol at −70 °C until use.

For the UV−vis absorption measurements, all spectra were obtained as described in I. The solvent used was a 10 mM phosphate buffer pH 7.0 diluted to 50 vol % with glycerol. The sample concentration was approximately 0.5 mM. A Hitachi U-3000 UV−vis spectrophotometer was used to measure the spectra. The effective slit width was 1 nm, and the sampling interval was 0.2 cm^{-1}. The temperature of the sample was varied using a top-loading OmniPlex cryostat (APD Cryogenics, Allentown, PA).[22] The path length of sample cell was 0.05 mm and CaF_2 windows were used. The spectral resolution was 0.1 nm. All spectra were deconvoluted using PeakFit (Jandel Scientific Software, CA).

The procedures for hole burning and examining the effect of an externally imposed electric field on the holes are described by Laberge et al.[45] The sample was held at 1.7 K, and the holes were burnt in the Q(0,0) absorption band using a ring dye laser (Coherent 899−211) pumped by a single-mode argon ion laser (Coherent Innova Sabre). After the hole spectrum was recorded, the electric field was varied in increments up to 22 kV/cm, and spectra were again taken. A discussion of field effects on hole burning is given by Kohler et al.[46]

Computational Modeling. Quantum chemical calculations utilized the INDO/s semiempirical method developed and parametrized for spectroscopy by Zerner and co-workers,[41,43,47] using the ZINDO program as implemented in the Cerius 2 software package (Molecular Simulations, Inc., Sherrills Ford, NC). Single-configuration interaction (SCI) was used in conjunction with the INDO/s method to calculate optical spectra. Excitations from 59 occupied to 59 unoccupied molecular orbitals were included in the SCI calculation.

Electrostatics calculations on the protein and surrounding solvent were performed using the software package DelPhi[48−51] as applied in our earlier work on heme containing proteins.[10,11,17,52] These calculations obtain finite difference solutions to the Poisson−Boltzmann equation:

$$\nabla\cdot[\epsilon(\mathbf{r})\nabla\phi(\mathbf{r})] - \kappa(\mathbf{r})^2\epsilon(\mathbf{r})\sinh[\phi(\mathbf{r})] = -4\pi\rho(\mathbf{r})/k_B T \quad (1)$$

where $\phi(\mathbf{r})$ is the electrostatic potential in units of k_BT/e (k_B is the Boltzmann constant, T is the absolute temperature, and e is the elementary charge unit), $\epsilon(\mathbf{r})$ is the (position dependent) dielectric constant, $\rho(\mathbf{r})$ is the fixed charge density (in units of e), and $\kappa(\mathbf{r})$ is the Debye−Hückel constant, which is proportional to the square root of the ionic strength: $\kappa(\mathbf{r})^2 8\pi e^2 I/\epsilon(\mathbf{r})k_BT$. In the absence of mobile ions, $\kappa(\mathbf{r}) = 0$ everywhere and eq 1 reduces to the Poisson equation.

A two-dielectric model is used for the protein−solvent system, with the dielectric boundary defined by the molecular surface of the protein. The interior (protein) dielectric constant was assumed to be 4, which accounts for the electronic polarizability of the protein. The exterior (solvent) dielectric constant was taken to be 80, although we found that the results were not particularly sensitive to the exact value chosen. Parameters used in the finite difference (FDPB) calculations were as follows: grid dimensions were 65 in each direction, with a scale of about 1.1 grids/Å. The ionic strength used was 0.1, to approximately correspond with the experimental phosphate buffer conditions. Solutions were obtained for the linear Poisson−Boltzmann equation with Debye−Hückel type boundary conditions, using the multigrid method of iteration combined with dielectric smoothing and charge anti-aliasing, with a final

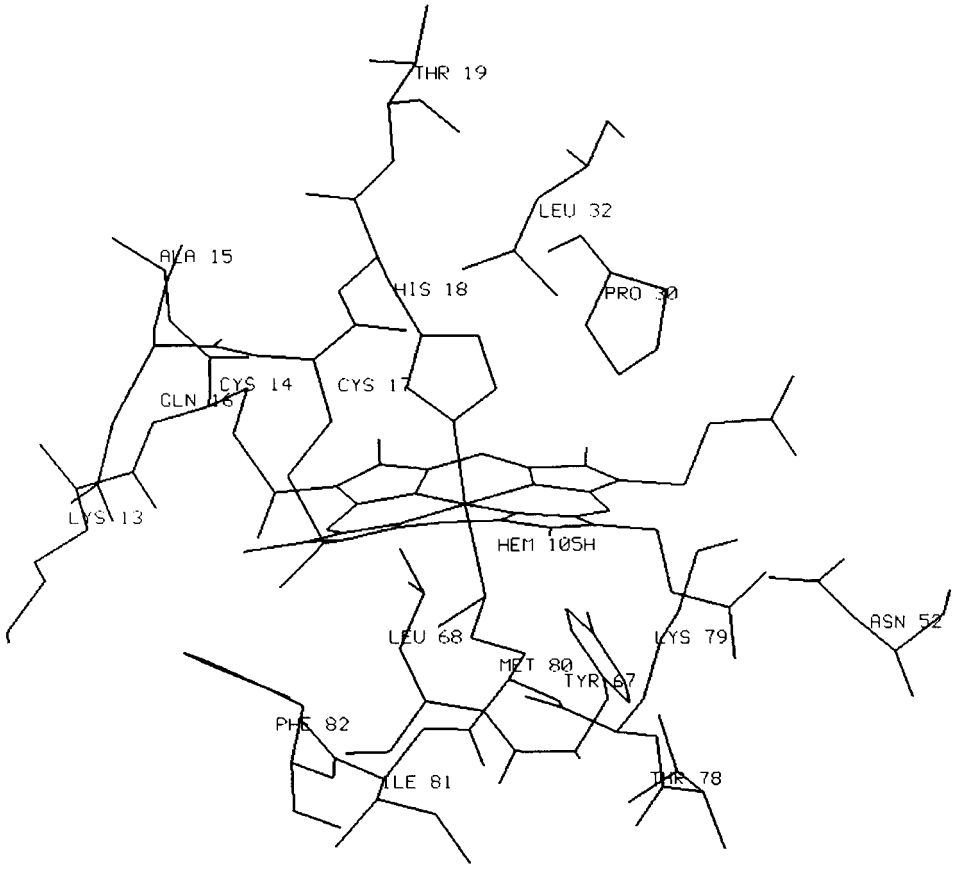

Figure 1. Heme and surrounding amino acids. Selected residues within approximately 8 Å of the central metal of the heme are shown.

convergence value of 1×10^{-4} *kT*/*e* total residual error in the potential. For the protein charges, a formal charge set was used in which charges were assigned according to the most likely protonation state of each residue at the experimental pH,[53] In this charge set, a charge of +0.5 was assigned to the NH1 and NH2 Arg nitrogens and +1.0 was assigned to the Lys NZ nitrogen. In addition, a charge of −0.5 was assigned to the OD1 and OD2 Asp oxygens, the OE1 and OE2 Glu oxygens, and also to the oxygens of the heme propionates. Other heme atoms were not assigned any charge since they are treated explicitly in ZINDO. To determine the ionization state of the propionates, FDPB calculations of their pK_a's were performed using the method of Yang et al.[54] These calculations show that although the propionates are buried, significant stabilization of the ionized form comes from the surrounding polar groups, such that the pK_a of the propionate from porphyrin pyrole group A is actually lowered, and thus it is charged (deprotonated at experimental pH). The propionate from pyrole group D has a pK_a of about 4−5, and hence is also likely to be charged at pH 7. The above charge assignment scheme was chosen to take into account the major contributions to the electric field imposed on the porphyrin ring of the heme group by the protein.

Coordinates for cytochrome *c* were taken from the entries 1HRC,[55] 5CYT,[56] and 1YCC[57] of the Research Collaboratory for Structural Bioinformatics for horse heart (HH), tuna heart (TH), and yeast (Y) cyt *c*, respectively. Hydrogens were added and the heme iron was replaced with zinc using the Biopolymer module of the Insight II software package (Biosym Technologies, San Diego, CA). Figure 1shows the heme group of HH Fe(II) cyt *c* along with some surrounding amino acids. The porphyrin ring is covalently bound to the protein via thioether linkages to the cys14* and cys17* residues, and the Fe is axially coordinated by his18† and met80†.

The electrostatic field generated by the protein is incorporated into the quantum mechanical calculation of the spectra as follows. After solutions to the Poisson−Boltzmann equation are obtained, the electrostatic potential ϕ_i and field components, E_i^x at the *m* atomic centers of the porphyrin ring of the heme are fitted by a set of *n* "virtual" point charges placed uniformly on the surface of a sphere surrounding the heme, where the magnitudes of the point charges q_j are given by the solution to the matrix equation

$$\mathrm{R}_{jl} q_j = \mathbf{Y}_l \tag{2}$$

$\mathbf{Y}_l$ is a 4*m* element vector, and $\mathbf{R}_{jl}$ is an $4m \times n$ matrix, whose elements are given by

$$\begin{aligned}
&\mathbf{Y}_l = \phi_i \quad \mathbf{R}_{jl} = \frac{1}{|\mathbf{r}_i - \mathbf{r}_j|} \quad 1 = i, \quad \text{for } i = l, m \\
&\mathbf{Y}_l = E_i^x \quad \mathbf{R}_{jl} = \frac{x_i - x_j}{|\mathbf{r}_i - \mathbf{r}_j|^3} \quad 1 = i + m, \quad \text{for } i = 1,m \\
&\mathbf{Y}_l = E_i^y \quad \mathbf{R}_{jl} = \frac{y_i - y_j}{|\mathbf{r}_i - \mathbf{r}_j|^3} \quad 1 = i + 2m, \quad \text{for } i = 1,m \\
&\mathbf{Y}_l = E_i^z \quad \mathbf{R}_{jl} = \frac{z_i - z_j}{|\mathbf{r}_i - \mathbf{r}_j|^3} \quad 1 = i + 3m, \quad \text{for } i = 1,m
\end{aligned} \tag{3}$$

where $\mathbf{r}_i$ and $\mathbf{r}_j$ are the coordinates of the atomic centers and the virtual charges, respectively. Choosing $n > 4m$ yields an over-determined set of equations which can be solved using a singular value decomposition routine[58] to provide an exact fit to the potentials and fields to within the numerical precision.

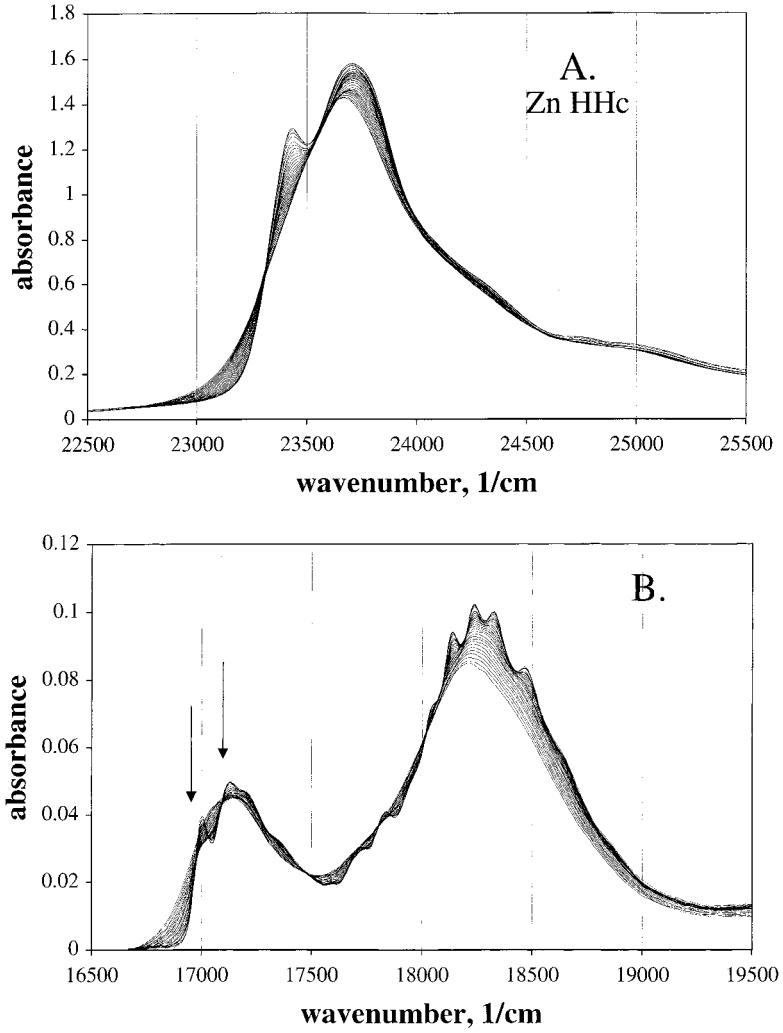

Figure 2. Absorption spectra for horse heart Zn cyt *c*. A. Soret region. B. Visible or Q(0,0) region. The spectra were recorded from higher (290 K) to lower temperature (10 K) in increments of 10 degrees. The lower, least resolved spectra are for the higher temperature. Sample conditions given in Materials and Methods. Arrows indicate the frequencies used for the hole burning experiment described in Figure 5.

The Coulombic potential produced by the resulting virtual charge set (q_j,$\mathbf{r}_j$) contains exactly the same information about potentials and fields at the heme atomic centers as that provided by the FDPB solutions, which account for protein charge, solvent polarization and ionic atmosphere screening. This virtual charge method enabled us to readily introduce the protein field into the quantum mechanical calculation, since the "classical" charges possess no basis functions and are thus included in the Fock matrix as a Coulombic potential, without adding any significant computational time. Providing $n > 4$m, there is no unique solution for (q_j,$\mathbf{r}_j$) so we are free to pick n and $\mathbf{r}_j$ for numerical convenience. Good results were obtained with $n =$ 850, where the sphere radius is determined by introducing a buffer zone of 3 Å, which gives the smallest distance allowable between any atom of the heme and any virtual charge.

III. Low Temperature UV−Vis Absorption Spectrum of Zn Cyt *c*

The Soret and Q-band regions of the UV−vis absorption spectra for Zn HH, TH, and Y cyt*c* are shown at temperatures ranging from 270 to 10 K in Figures 2−4, respectively. The room-temperature spectra are typical of that closed subshell transition metallo-porphyrins.[18] As the temperature is lowered below approximately 180 K, both the Q(0,0) and B(0,0) bands begin to show clear signs of splitting. At temperatures below 100 K, these splittings are well resolved for the horse and tuna proteins (Figures 2 and 3), and also split for the yeast protein (Figure 4). The splittings based upon spectral deconvolution of the Q and Soret bands for HH, TH, and Y Zn cyt *c* at 10 K are given in Table 1. We point out that both the Q and Soret splittings for Zn cyt *c* follow the same trend as the Q-band splitting for Fe(II) cyt *c* when comparing different species. The Q-band splittings for Zn cyt *c* are approximately the same magnitude as that of Fe(II) cyt *c* (the Q-band splittings for Zn cyt *c* are slightly larger).

TABLE 1. Q(0,0) and Soret Band Transition Energies and Splittings Observed for Zn Cyt *c* at 10 K

	peak 1 (cm^{-1})	peak 2 (cm^{-1})	splitting (cm^{-1})
Zn cyt *c*			
HH Q(0,0) band	16998	17118	122
TH Q(0,0) band	17007	17125	118
Y Q(0,0) band	17127	17230	103
HH Soret band	23400	23696	296
TH Soret band	23413	23667	254
Y Soret band	23596	23793	197
Fe(II) cyt *c*[22]			
HH Q(0,0) band	18256	18375	119
TH Q(0,0) band	18267	18371	104
Y Q(0,0) band	18274	18353	80

As discussed in I[22] and in the Introduction, the general explanation for such band splittings is that the asymmetric heme

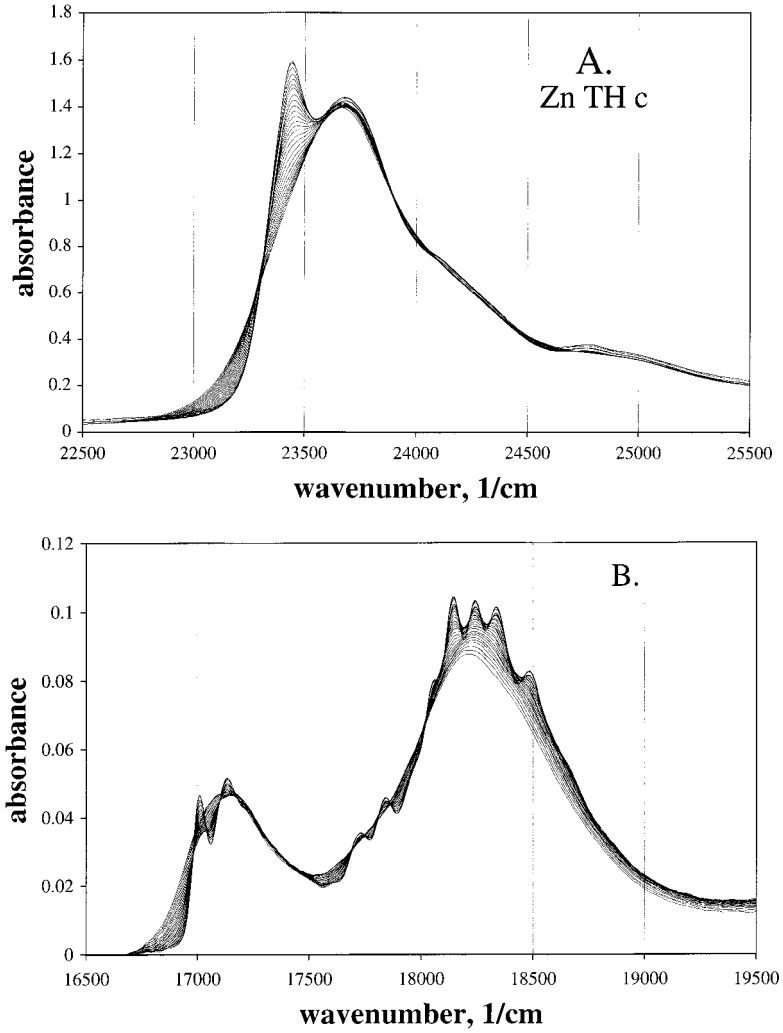

Figure 3. Absorption spectra for tuna heart Zn cyt *c*. A. Soret region. B. Visible or Q(0,0) region. The spectra were recorded from higher (290 K) to lower temperature (10 K) in increments of 10 degrees. The lower, least resolved spectra are for the higher temperature. Sample conditions given in Materials and Methods.

pocket environment somehow removes the 2-fold degeneracy of the Q(0,0) transition. The electrostatic influence of the protein on the porphyrin ring of the heme group can be viewed in terms of a multipolar expansion of the electrostatic potential energy. This was discussed in detail in I. Therefore, we will only summarize the results here, and refer the reader to I for a more complete discussion. Essentially, the interaction of the porphyrin ring with the uniform component of the internal field, given by the dipolar term in the expansion, leads to a splitting given approximately by

$$\Delta = \sqrt{(\epsilon/2)^2 + (\mu E)^2} - \epsilon/2 \approx (\mu E)^2/\epsilon \qquad (4)$$

where E is the internal electric field strength, ϵ is the energy of the transition, and μ is the transition dipole moment. Thus, the greater the internal field and/or the more intense the transition, the greater the protein induced splitting of the absorption band. Given the fact that the Q-band of cyt *c* is very weak, we found that the large internal field strength of roughly 10−15 MV/cm was simply not great enough to lead to the splittings observed, only contributing about 10 cm^{-1} to the Q(0,0) splitting. However, we did find that the quadrupole term (the next interaction term in the multipolar expansion), combined with a protein induced distortion of the porphyrin ring, is capable of leading to the observed splittings of approximately 100 cm^{-1}. Since the Soret band is much more intense, one might expect the induced splitting due to the dipolar term to be much larger, possibly contributing hundreds of cm^{-1} to the splitting. However, there did not appear to be a resolved splitting for Fe(II) cyt *c* in I.

Since the line widths in Zn cyt *c* are narrower and the Soret band is more intense than that of Fe(II) cyt *c*,[44] we are able to observe a resolved Soret splitting. While the Q(0,0) splitting for HH, TH, and Y Zn cyt *c* is approximately the same as the corresponding Q(0,0) splittings in Fe(II) cyt *c*, the Soret splittings are approximately two times as large as the Q(0,0) splittings. This is consistent with a larger uniform field contribution to the splitting. Using E = 13 MV/cm, ϵ_Q = 18000 cm^{-1}, ϵ_B = 24000 cm^{-1}, μ_Q = 3 D, and μ_B = 10 D (yielding a Soret:Q intensity ratio of about 10:1, which is what we observe experimentally), we obtain uniform field induced splittings of Δ_Q = 14 cm^{-1} and Δ_B = 117 cm^{-1}. When these numbers are combined with the higher order field-induced splittings and distortion induced splitting discussed in the first part of this series (ref 22), it is possible to obtain calculated splittings that are consistent with the experimental splittings given in Table 1.

IV. Stark Effect Holeburning Spectra of Zn Cyt *c*

Horse Heart Zn cyt *c*. The Stark effect hole-burning spectrum of HH Zn cyt *c* is shown in Figure 5A−D. The lighter

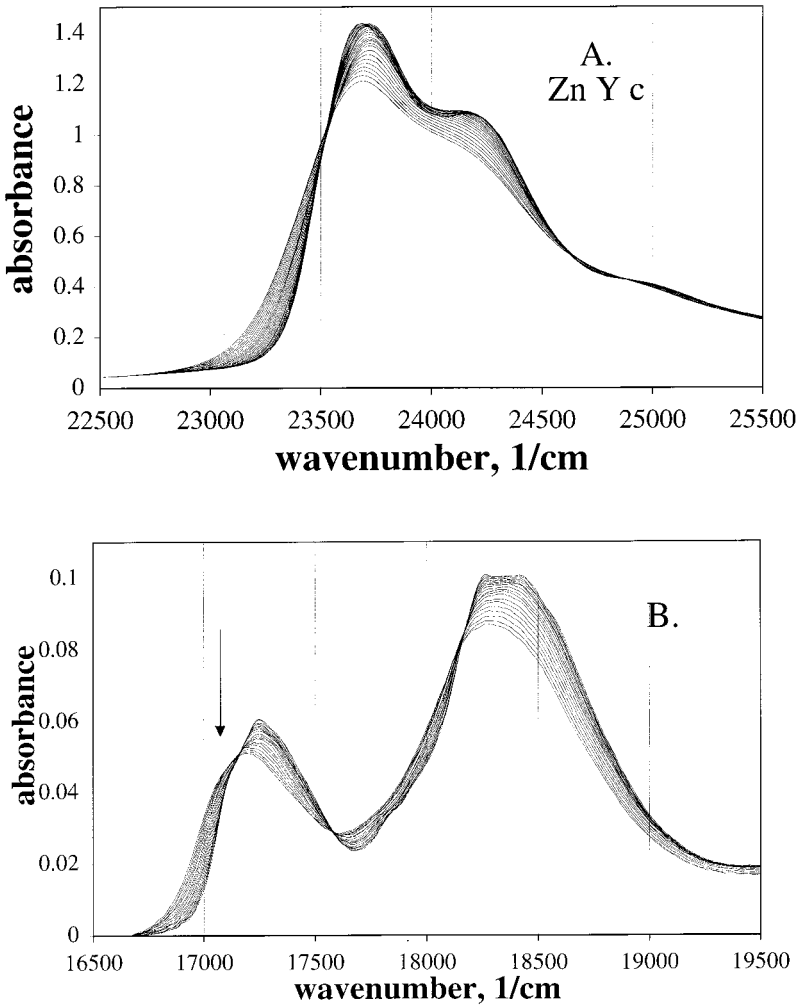

Figure 4. Absorption spectra for yeast Zn cyt *c*. A. Soret region. B. Visible or Q(0,0) region. The spectra were recorded from higher (290 K) to lower temperature (10 K) in increments of 10 degrees. The lower, least resolved spectra are for the higher temperature. Sample conditions given in Materials and Methods. Arrow indicates the frequency used for the hole-burning experiment described in Figure 5.

lines show the holes before application of an electric field; the darker lines are after a field was applied. In previous studies,[11,13,45] due to the ability to efficiently burn narrow holes in both components of the split Q-band, it was inferred that distinct protein conformations existed "under" each of the Q-band components. For a single conformation, rapid relaxation from the upper Q_y to the lower Q_x state should prevent efficient narrow holeburning (i.e., hole width < 1 GHz) in the upper component. This has also been pointed out for Mg-mesoporphyrin embedded in horseradish peroxidase[26,59] and for aluminum phthalocyanine in a glassy matrix.[60] However, it has been argued that if two conformations are present, e.g., a "blue" higher energy conformation and a "red" lower energy conformation,[45] it is possible that the Q_x band of the blue conformer overlaps the Q_y band of the red conformer. In this case, apparent narrow holeburning should be observed in the Q_y band. In reality, many conformations are likely to be present. As long as some significant part of the inhomogeneously broadened Q_x band overlaps with the inhomogeneously broadened Q_y band, then apparent narrow holeburning should be possible in the Q_y band. This has served as an explanation for the ability to burn narrow holes in both of the peaks shown in Figure 5A−D.

It has also been pointed out that the behavior of the two holes in an electric field is different. When an electric (Stark) field, E_{St}, is applied parallel to the polarization of the probing laser field, E_L, the red hole splits (Figure 5C). Under perpendicular polarization, the hole simply broadens symmetrically (Figure 5D). This is characteristic of a chromophore that has a permanent dipole moment, which in this case is induced by the protein (since an idealized porphyrin ring is centrosymmetric). Upon excitation of the chromophore, this dipole moment typically changes, leading to a dipole moment difference vector $\Delta\mu$. The splitting under parallel polarization is also an indication that the angle φ between the transition dipole and $\Delta\mu$ for this transition is less than 55°. There will also typically be a change in polarizability of the chromophore $\Delta\tilde{\alpha}$ upon excitation. If only two electronic levels are considered for each molecule, within an inhomogeneously broadened absorption band the transition energies of the individual absorbers will then undergo a frequency shift given by

$$\Delta\nu = -\frac{1}{h}\left(\Delta\mu\cdot\mathbf{E} + \frac{1}{2}\mathbf{E}\Delta\tilde{\alpha}\mathbf{E}\right) \qquad (5)$$

The first term in parentheses in eq 5 is linear in the applied field **E** and is typically much larger than the second term, which is quadratic in **E**, when the chromophore has a significant dipole moment. When the chromophore has an effective center of symmetry, the quadratic term becomes much more important.

When a narrow hole is burnt in a randomly oriented sample, the linear term will change sign when the direction of **E** reverses with respect to $\Delta\mu$. This is what leads to the splitting of a hole in an external field, and a symmetric profile of the hole-burning spectrum under an applied field.[46,61] We also point out that, the larger $\Delta\mu$ is for a given value of **E**, the larger the splitting.

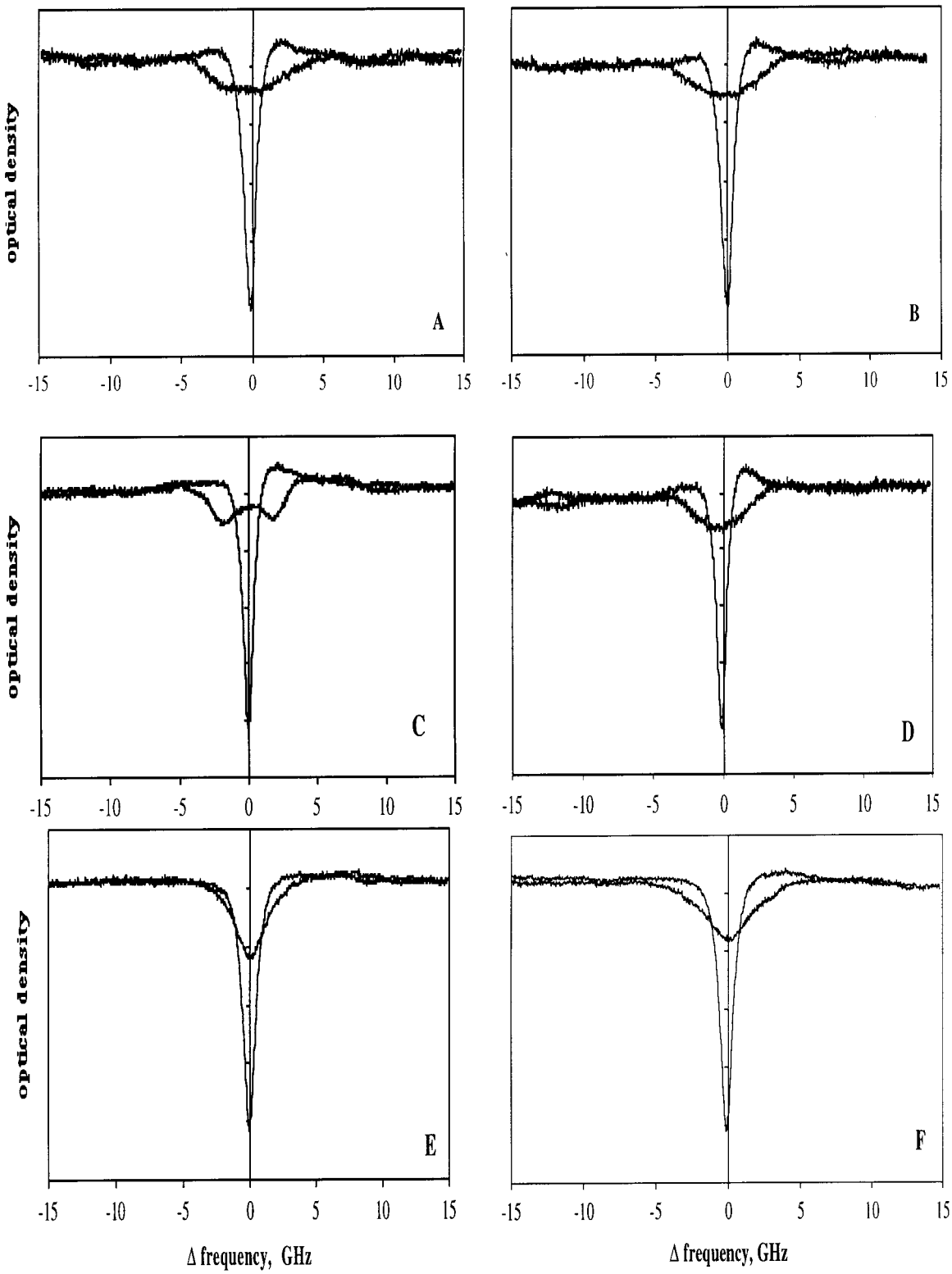

Figure 5. Stark Effect Hole burning spectra. Conditions given in Laberge et al.[45] In the left panels (A, C and E), E_L was parallel to E_{St}. In the right parts (B, D, and F), E_L was perpendicular to $E_{St.}$ Light lines show the hole spectra before application of electric field; dark lines show the hole after application of the field of 22 V/cm. A, B. Hole burned in HH Zn cyt *c* at 17113 cm^{-1}, C, D. Hole in HH Zn cyt *c* burned at 16990 cm^{-1}. To see where this is on the absorption spectrum, see Figure 2B. E,F. Hole burned in Y Zn cyt *c*. The hole frequency was at 17116 cm^{-1}. To see where this is on the absorption spectrum, see Figure 4B.

For the blue component, the hole exhibits a flattening (Figure 5B), suggestive of an unresolved splitting, when the Stark field is applied perpendicular to the polarization of the probing laser field. This would be an indication that the angle φ between the transition dipole and $\Delta\mu$ for this transition is greater than 55°. However, there could also be an unresolved splitting under parallel polarization, since it is difficult to distinguish between an unresolved splitting and a simple broadening of the hole.

Yeast Zn cyt *c*. The Stark effect holeburning spectrum of Y Zn cyt *c* is shown in Figure 5E and F. In contrast to HH Zn cyt *c*, narrow hole-burning is only possible in the red component of the Q-band. It has been suggested on this basis that Y Zn

cyt *c* is less "disordered" than HH Zn cyt *c*, having only one distinct conformation.[45] Molecular dynamics studies further suggested that HH Zn cyt *c* explores a greater region of conformational space than does Y Zn cyt *c*, consistent with the holeburning results. As was the case for the blue conformation of HH Zn cyt *c*, the hole exhibits stronger broadening under perpendicular polarization, indicating a possible unresolved splitting (compare Figure 5F with E). Again, this would also indicate that the angle φ between the transition dipole and $\Delta\mu$ for this transition is greater than 55°. Thus, it has been implied[45] that this conformation is similar to that of the blue conformation of HH Zn cyt *c*.

V. Calculation of the Protein Induced Polarization of the Zn−Porphyrin Ring

To give a more quantitative description of the difference between the heme pocket environment of HH and Y Zn cyt *c*, we performed INDO/s-SCI calculations on the porphyrin ring of the heme group for these two proteins. The protein electrostatic field, computed from Poisson−Boltzmann electrostatics, was included in the calculation as virtual point charges, as discussed in the Materials and Methods Section. We performed two sets of calculations: one in which the axial histidine and methionine are included in the quantum mechanical part of the calculation, and one in which only the porphrin ring is used. We did not find significant differences in the calculated absorption spectra. This is presumably because Zn^{2+} is a d^{10} transition metal, and strong field axial ligation is not required to stabilize the singlet ground electronic state, as it is for Fe^{2+}. For this reason, and since we are interested primarily in how the protein affects the electronic structure of the porphyrin ring itself, we focus on the porphyrin ring-only calculations below. Furthermore, we are interested mainly in the induced dipole moment of the ground and first electronic excited states of the porphyrin ring, since these vectors and their relationship to the transition dipole moment are the main determinant of whether a hole splits in an applied electric field. This justifies our use of a formal charge set, since it was shown in I that the polar groups give a contribution to the electrostatic potential that is nearly centrosymmetric within the plane of the porphyrin ring. Therefore, this contribution is not expected to induce a significant dipole moment in the π-electron system of the porphyrin ring.

The INDO/s-SCI method yields a representation of the porphyrin UV−vis absorption spectrum that reproduces the overall experimental features (see Table 2). The calculated energies of the Q and Soret transitions are lower and higher, respectively, than is observed experimentally. The overestimation of the Soret band energy is likely to be a result of problems associated with the SCI method.[62] The underestimation of the Q-band energy may be due to the bond lengths used in the calculation, which were taken directly from the PDB files used. Similar low transition energies were obtained in an INDO/s-SCI study of aluminum phthalocyanine complexes.[60]

The Q-band calculated splittings are 149 and 108 cm^{-1} in the presence and absence of the electric field for HH cyt *c*. These respective values are 592 and 590 cm^{-1} for Y cyt *c*. While these are of the correct order of magnitude, it is perhaps unreasonable to expect this method to predict more accurate splittings on the basis of porphyrin ring distortion and electrostatic effects, at least without additional parametrization. For example, the large splitting for Y Zn cyt *c* may be a consequence of the bond lengths in the structure taken directly from the PDB entry, as discussed above. Although one could attempt minimizing the entire protein using various molecular mechanics force fields to see if the splitting for Y Zn cyt *c* could be better reproduced, we did not feel that this was the appropriate direction to take. As pointed out by Shelnutt and co-workers[3,6,63] the heme conformation is approximately conserved when comparing the X-ray structures of cyt *c* from different species. Therefore, the differences in structure between the heme groups of Y and HH cyt *c* are subtle. If molecular mechanics minimization did lead to a more accurate calculated splitting, this could be interpreted in one of two ways. If the minimized structure were significantly different from the X-ray structure, the results would clearly not be representative of the actual protein conformation. On the other hand, if the minimization led to only a slight change in the structure, this would indicate that the heme is exploring a region of the INDO/s-SCI energy surface for which the calculated excitation energies are very sensitive to conformation. In other words, the "slope" of the energy surface would be large. This suggests that the quantum mechanical method, with its current parametrization, is unable to account for distortions in the molecular structure well enough to reproduce the observed splittings. Nevertheless, the accuracy of the INDO/s-SCI method is adequate for our purposes here, since we are mainly interested in the degree to which the porphyrin ring is polarized in the protein. The electric field seems to have more of an effect on the splitting for the HH protein than for Y cyt *c*. The main effect with Y cyt *c* is to blue shift both the Q_x and Q_y bands by roughly the same amount, such that there is only a small effect on the Q_x, Q_y splitting.

TABLE 2. INDO/s-SCI−PB Calculated Dipole Moment Parameters for the Lowest Energy Q(0,0) Transition and Calculated Spectral Splittings and Energies of HH and Y Zn Cyt *c*

	HH Zn cyt *c*	Y Zn cyt *c*
$\lvert\mu_Q\rvert$ (Debye)	3.43	3.84
$\lvert\Delta\mu\rvert$ (Debye)	0.59	0.46
ϕ (degrees)	31.3	48.4
Q(0,0) splitting and energies without protein field, cm^{-1}	108 (14812, 14704)	590 (15201, 14611)
Q(0,0) splitting and energies with field, cm^{-1}	149 (14851, 14702)	592(15214, 14622)
Soret splitting and energies without protein field, cm^{-1}	197 (26963, 26766)	220 (26678, 26458)
Soret splitting and energies with protein field, cm^{-1}	248 (26958, 26710)	260 (26656, 26396)

Table 2 gives the calculated values of $|\Delta\mu|$, the magnitude of the transition dipole moment $|\mu_Q|$, and the angle φ between them for HH and Y Zn cyt *c*, along with the calculated splittings with and without the electric field. The dipole moment difference for HH Zn cyt *c* is greater than that of Y Zn cyt *c*. Since the contribution to the linear Stark shift of a transition is also linear in $\Delta\mu$, one would expect a greater likelihood that a hole in the absorption spectrum would split. Furthermore, the predicted angle φ for HH Zn cyt *c* is 31.3°, which is considerably less than the 55° required for the hole to split under parallel polarization of the applied and probing fields. The hole was observed to split under these conditions (Figure 5C), consistent with the calculations. We point out that, while φ is still predicted to be less than 55° for Y Zn cyt *c*, the calculated value of 48.4° is much closer to 55° than for HH Zn cyt *c*. Thus, the hole burnt in the Q-band of Y Zn cyt *c* might be expected not to

exhibit splitting under either parallel or perpendicular polarization, which is also consistent with the experimental observations (Figure 5E).

Finally, although the protein electrostatic field increases the dipole moment difference for both HH and Y Zn cyt *c*, the amount of the increase is essentially the same for these two proteins (0.15 D for HH and 0.14 D for Y). The primary difference appears to be due to the way the protein distorts the porphyrin ring. The protein field also acts to decrease the angle φ between $\Delta\mu$ and μ_Q for both HH and Y Zn cyt *c*. This effect is much greater for Y than for HH, with φ being reduced from 146.6° to 48.4° for Y Zn cyt *c*, and from 48.2° to 31.3° for HH Zn cyt *c*.

VI. Discussion and Conclusions

In this paper, we demonstrated that the magnitude of the low-temperature Q(0,0) band splitting observed in Zn substituted cyt *c* from horse heart, tuna heart, and yeast follows the same trend as in the native Fe(II) proteins. Furthermore, we showed that the Soret band of the Zn substituted protein also shows a significant splitting at low temperature, and that this splitting follows the same trend as that of the Q(0,0) band. We suggested that the Soret splitting is unresolved in the Fe(II) proteins due to the faster decay times, leading to larger line widths in the low temperature absorption spectrum. If this is the case, then it is likely that the mechanism for the splittings observed in Zn cyt *c* is the same as suggested in I [22] to be responsible for the Q(0,0) splittings of Fe(II) cyt *c*. This supports our use of the Zn substituted protein to help understand the protein−heme interactions in the native protein.

The large magnitude of the Soret splitting compared to the Q(0,0) splitting of Zn cyt *c* was shown to be consistent with a uniform electric field model of the heme pocket environment. *Variations* in the uniform component of the field did not seem to be responsible for the variations in the Q(0,0) band splitting across different species, as shown in I. The finding that the Soret peak is split highlights the fact that the large magnitude of this component of the field contributes significantly to alterations in the porphyrin ring electronic structure.

The Stark effect of photochemical holes burnt in the Q(0,0) region of HH and Y Zn cyt *c* was used to further study the differences in the heme pocket environments of the two proteins. Laberge et al.[45] argued that the ability to burn holes in both of the Q(0,0) components of HH Zn cyt *c* suggests that a distinct conformation of the protein exists for which the Q_x band occurs at a higher energy, such that it overlaps the Q_y band of another "main" conformation. Considering Table 1, the upper Q(0,0) component of HH Zn cyt *c* peaks at about the same energy as the lower Q(0,0) component of Y Zn cyt *c*. Laberge et al. used this observation, along with the similarity of the holes burnt into the upper Q(0,0) component of HH Zn cyt *c* to that of the hole burnt into the lower Q(0,0) component of Y Zn cyt *c*, to suggest that the second conformation of HH Zn cyt *c* has a similar heme pocket environment to Y cyt *c*. If this is indeed the case, then examination of how the protein perturbs the porphyrin ring of the heme group for both proteins should provide insight into the nature of the proposed second conformation of HH Zn cyt *c*.

INDO/s calculations on the Zn−porphyrin ring with the rest of the protein represented as virtual point charges demonstrated that the protein electrostatic field does increase the value of $|\Delta\mu|$, but it does so by about the same amount for both HH and Y Zn cyt *c*. This makes sense, since the induced dipole moment is more sensitive to the uniform component of the field than higher order components, and since the uniform component of the field is very similar for HH and Y Zn cyt *c*. The effect on the induced dipole moment is different than on the splitting of the degeneracy of the bands, which can be quite sensitive to higher order moments, and more or less sensitive to the uniform component depending on the intensity of the band.

The primary difference in $|\Delta\mu|$ appears to be due to differences in the protein induced distortion of the porphyrin ring from D_{4h} symmetry. This is consistent with the molecular dynamics studies of Laberge et al.[45] which showed that the heme group in HH Zn cyt *c* explores a greater region of conformational space than its Y Zn cyt *c* counterpart. Therefore, it is likely that the region of conformational space explored by the porphyrin ring of HH cyt *c* overlaps that of the Y Zn cyt *c* structure, with a structure that possesses the same or similar $\Delta\mu$ and μ_Q, as well as a similar absorption spectrum.

The electrostatic field does tend to strongly modify the angle φ between $\Delta\mu$ and μ_Q, such that φ is much closer to 55° for Y Zn cyt *c*. This is also consistent with the experimental result that the hole burnt into the Q_x band of Y Zn cyt *c* does not show resolved splitting under either parallel or perpendicular polarization of the applied and probing fields.

We should point out areas in our analysis where possible improvement can be made. SCI is only a first approximation in calculating excited state properties, much the way HF is a first approximation in calculating ground state properties. Therefore, multiply excited configurations may alter the results significantly. We further assumed that the replacement of Fe by Zn did not significantly alter the structure of the protein, a supposition that can be tested by structure determination. Our study does pave the way to a general methodology for incorporating protein electric fields into semiempirical quantum chemical calculations of prosthetic groups. This modeling will help us to put high-resolution spectroscopic experiments, such as Stark-effect hole burning, on a more quantitative level, hopefully yielding detailed and predictive information about how the protein interacts with the prosthetic group.

Acknowledgment. The National Institute of Health Grants PO1 GM48310 and R01 GM55004 supported this work.

Abbreviations

cyt *c* = cytochrome *c*
HH = horse heart
Y = yeast
TH = tuna

References and Notes

(1) Ma, J.-G.; Laberge, M.; Song, Z.-Z.; Jentzen, W.; Jia, S.-L.; Vanderkooi, J. M.; Shelnutt, J. A. *Biochemistry* **1997**, *37*, 55118-5128.

(2) Ma, J.-G.; Jentzen, W.; Laberge, M.; Vanderkooi, J.; Song, X.-Z.; Jia, S.-L.; Hobbs, J. D.; Shelnutt, J. *Biophys. J.* **1997**, *72*, A10.

(3) Hobbs, J. D.; Shelnutt, J. A. *J. Protein Chem.* **1995**, *14*, 19−25.

(4) Shelnutt, J. A.; Rousseau, D. L.; Dethmers, J. K.; Margoliash, E. *Biochemistry* **1981**, *20*, 6485−6497.

(5) Shelnutt, J. A.; Rousseau, D. L.; Dethmers, J. K.; Margoliash, E. *Proc. Natl. Acad. Sci. U.S.A.* **1979**, *76*, 3865−3869.

(6) Jentzen, W.; Ma, J.-G.; Shelnutt, J. A. *Biophys. J.* **1998**, *74*, 753−763.

(7) Jentzen, W.; Simpson, M. C.; Hobbs, J. D.; Song, X.; Ema, T.; Nelson, N. Y.; Medforth, C. J.; Smith, K. M.; Veyrat, M.; Mazzanti, M.; Ramasseul, R.; Marchon, J.-C.; Takeuchi, T.; Goddard, W. A. I.; Shelnutt, J. A. *J. Am. Chem. Soc.* **1995**, *117*, 11085−11097.

(8) Barkigia, K. M.; Renner, M. W.; Furenlid, L. R.; Medforth, C. J.; Smith, K. M.; Fajer, J. *J. Am. Chem. Soc.* **1993**, *115*, 3627−3635.

(9) Geissinger, P.; Kohler, B. E.; Woehl, J. C. *J. Phys. Chem.* **1995**, *99*, 16527−16529.

(10) Laberge, M.; Sharp, K. A.; Vanderkooi, J. M. *Biophys. Chem.* **1998**, *71*, 9−20.
(11) Laberge, M.; Sharp, K. A.; Vanderkooi, J. M. *J. Phys. Chem. B* **1997**, *101*, 7364−7367.
(12) Laberge, M.; Vanderkooi, J. M.; Sharp, K. A. *J. Phys. Chem.* **1996**, *100*, 10793−10801.
(13) Köhler, M.; Gafert, J.; Friedrich, J.; Vanderkooi, J. M.; Laberge, M. *Biophys. J.* **1996**, *71*, 77−85.
(14) Lockhart, D. M.; Kim, P. S. *Science* **1992**, *257*, 947−951.
(15) Honig, B.; Nicholls, A. *Science* **1995**, *268*, 1144−1149.
(16) Geissinger, P.; Kohler, B. E.; Woehl, J. C. *Synth. Met.* **1997**, *84*, 937−938.
(17) Anni, H.; Vanderkooi, J. M.; Sharp, K. A.; Yonetani, T.; Hopkins, S. C.; Herenyi, L.; Fidy, J. *Biochemistry* **1994**, *33*, 3475−3486.
(18) Gouterman, M. *The Porphyrins*; Academic Press: New York, 1978; pp 1−156.
(19) Herenyi, L.; Fidy, J.; Gafert, J.; Friedrich, J. *Biophys. J.* **1995**, *69*, 577−582.
(20) Wagner, G. C.; Kassner, R. J. *Biochem. Biophys. Res. Commun.* **1975**, *63*, 385−391.
(21) Friedman, J. M.; Rousseau, D. L.; Adar, F. *Proc. Natl. Acad. Sci. U.S.A.* **1977**, *74*, 2607−2611.
(22) Manas, E.; Vanderkooi, J. M.; Sharp, K. *J. Phys. Chem.* **1999**, *103*, 6334−6348.
(23) Wilson, D. F. *Arch. Biochem. Biophys.* **1967**, *121*, 757−768.
(24) Champion, P. M.; Collins, D. W.; Fitchen, D. B. *J. Am. Chem. Soc.* **1976**, *98*, 7114−7115.
(25) Reddy, K. S.; Angiolillo, P. J.; Wright, W. W.; Laberge, M.; Vanderkooi, J. M. *Biochemistry* **1996**, *35*, 12820−12830.
(26) Balog, E.; Kis-Petik, K.; Fidy, J.; Kohler, M.; Friedrich, J. *Biophys. J.* **1997**, *73*, 397−405.
(27) Hagihara, B.; Oshino, R.; Iizuka, T. *J. Biochem.* **1974**, *75*, 45−51.
(28) Cowan, J. A.; Gray, H. B. *Inorg. Chem.* **1989**, *28*, 4554−4556.
(29) Shelnutt, J. A. *J. Chem. Phys.* **1980**, *72*, 3948−3958.
(30) Schweingruber, M. E.; Sherman, F.; Stewart, J. W. *J. Biol. Chem.* **1977**, *252*, 6577−6580.
(31) Schweingruber, M. E.; Stewart, J. W.; Sherman, F. *J. Biol. Chem.* **1979**, *254*, 4132−4143.
(32) Angiolillo, P.; Vanderkooi, J. M. *Biophys. J.* **1995**, *68*, 2505−2518.
(33) Spiro, T. G.; Strekas, T. C. *Proc. Natl. Acad. Sci. U.S.A.* **1972**, *69*, 2622−2626.
(34) Valance, W. G.; Strekas, T. C. *J. Phys. Chem.* **1982**, *86*, 1804−1808.
(35) Shelnutt, J. A.; Cheung, L. D.; Chang, R. C. C.; Yu, N.-T.; Felton, R. H. *J. Chem. Phys.* **1977**, *66*, 3387−3398.
(36) Shibata, Y.; Kushida, K. *Chem. Phys. Lett. 284*, 115−120.
(37) Anni, H.; Vanderkooi, J. M.; Mayne, L. *Biochemistry* **1995**, *34*, 5744−5753.
(38) Zhou, J. S.; Kostic, N. M. *J. Am. Chem. Soc.* **1993**, *115*, 10796−10804.
(39) Zhou, J. S.; Kostic, N. M. *Biochemistry* **1993**, *32*, 4539−4546.
(40) Gouterman, M. *J. Mol. Spectrosc.* **1961**, *6*, 138−163.
(41) Bacon, A. D.; Zerner, M. C. *Theor. Chim. Acta* **1979**, *53*, 21−54.
(42) Zerner, M. C.; Loew, G. H.; Kirchner, R. E.; Mueller-Westerhoff, U. T. *J. Am. Chem. Soc.* **1980**, *102*, 589−599.
(43) Ridley, J.; Zerner, M. C. *Theor. Chim. Acta* **1973**, *32*, 111−134.
(44) Vanderkooi, J. M.; Adar, F.; Erecinska, M. *Eur. J. Biochem.* **1976**, *64*, 381−387.
(45) Laberge, M.; Köhler, M.; Vanderkooi, J. M.; Friedrich, J. *Biophys. J.* **1999**, *77*, 3293−3304.
(46) Koehler, M.; Friedrich, J.; Fidy, J. *Biochim. Biophys. Acta* **1998**, *1386*, 255−288.
(47) Ridley, J. E.; Zerner, M. C. *Theor. Chim. Acta* **1976**, *42*, 223−236.
(48) Nicholls, A.; Honig, B. *J. Comput. Chem.* **1991**, *12*, 435−445.
(49) Jayaram, B.; Sharp, K. A.; Honig, B. *Biopolymers* **1989**, *28*, 975−993.
(50) Gilson, M.; Sharp, K.; Honig, B. *J. Comput. Chem.* **1988**, *9*, 327−335.
(51) Sharp, K.; Honig, B. *Annu. Rev. Biophys. Chem.* **1990**, *19*, 301−332.
(52) Laberge, M.; Sharp, K.; Vanderkooi, J. M. *Biophys. J.* **1996**, *70*, A223.
(53) Laberge, M.; Vanderkooi, J. M.; Sharp, K. A. *J. Phys. Chem.* **1996**, *100*, 10793−10801.
(54) Yang, A.-S.; Gunner, M. R.; Sampogna, R.; Sharp, K.; Honig, B. *Proteins* **1993**, *15*, 252−265.
(55) Bushnell, G. W.; Louie, G. V.; Brayer, G. D. *J. Mol. Biol.* **1990**, *214*, 585−595.
(56) Takano, T.; Dickerson, R. E. *J. Mol. Biol.* **1981**, *153*, 79−94 (95−115).
(57) Louie, G. V.; Brayer, G. D. *J. Mol. Biol.* **1990**, *214*, 527−555.
(58) Press, W.; Flannery, B.; Teukolsky, S.; Vetterling, W. *Numerical Recipes*; Cambridge University Press: New York, 1986.
(59) Herenyi, L.; Sauisalu, A.; Mauring, K.; Kis-Petik, K.; Fidy, J.; Kikas, K. *J. Phys. Chem. B* **1998**, *102*, 5932−5940.
(60) Reinot, T.; Hayes, J. M.; Small, G. J.; Zerner, M. C. *Chem. Phys. Lett. 299*, 410−416.
(61) Gottfried, D. S.; Steffen, M. A.; Boxer, S. G. *Biochim. Biophys. Acta* **1991**, *1059*, 76−90.
(62) Baker, J. D.; Zerner, M. C. *Chem. Phys. Lett. 175*, 1922−1196.
(63) Ma, J.-G.; Jentzen, W.; Laberge, M.; Vanderkooi, J.; Song, X.-Z.; Jia, S.-L.; Hobbs, J. D.; Shelnutt, J. *Biophys. J.* **1997**, *72*, A10.